Green Chemistry

PAPER

View Article Online
View Journal | View Issue



Cite this: *Green Chem.*, 2023, **25**, 5276

# Rapid dissolution of high concentration poly(3-hydroxybutyrate) using neoteric biosolvents: experiment and molecular dynamics simulation†

Joseph Kinyanjui Muiruri, ‡[a] Jayven Chee Chuan Yeo,‡[b] Tang Yuanting Karen,[b] Ke Li,[b] Enyi Ye,[a,b] Xian Jun Loh *[a,b] and Zibiao Li *[a,b,c]

Nature, especially in hot environments, triggers the phase change of the abundant metabolites in plants from solid to liquid as a survival mechanism. Therefore, taking cues from nature, these metabolites could have potential as green solvents for the dissolution of biopolymers. Because of their green credentials, plant-derived aromatic monoterpenoids have gained considerable attention for the extraction of bioactive compounds to replace toxic halogenated solvents. In this work, we report for the first time the fast dissolution of high concentration poly(3-hydroxybutyrate) (PHB) using carvacrol (5-isopropyl-2-methylphenol) – a plant metabolite – as a solvent. Remarkably, 20 wt% PHB was completely dissolved within 30 min at 100 °C, whereas a 10 wt% PHB dissolved in 21 min, and even faster dissolution for 1 wt%, 3 wt% and 5 wt% PHB. The carvacrol/PHB solution exhibited stability characterized by rheology measurements and the atomistic molecular dynamics (MD) simulations elucidate the mechanism behind carvacrol's rapid dissolution of PHB. Most importantly, the carvacrol solvent can be fully recovered by adding anti-solvents. Furthermore, the resultant highly viscous carvacrol/PHB solution could find applications in coating formulations, adhesives, and consumer care additives.

Received 8th March 2023,
Accepted 25th May 2023

DOI: 10.1039/d3gc00793f

rsc.li/greenchem



## Introduction

Plastic – an oil-based material – has transformed human life in social, industrial, and environmental facets.[1] These oil-based polymers have dominated the plastic industry over time, and their dominance is entrenched by the fact that oil-based plastics are durable and exhibit exceptional mechanical performance.[2] Unfortunately, populations have morphed over the years into a 'use and throw-away' society that has clogged the environment due to plastic pollution.[3] This pollution problem has roused researchers into an unprecedented search for eco-friendly alternatives. This search has identified some exciting biopolymers, such as poly(hydroxyalkanoates) (PHA), which are processed by microbes under a nutrient famine-phase and excess carbon substrate glut-phase as carbon and energy storage granules.[4,5] The extracted polymers from these granules exhibit good biocompatibility and biodegradability features with potential applications in medical and sustainable packaging industries.[6]

PHAs, such as poly(hydroxybutyrate) (PHB) or poly(3-hydroxybutyrate-*co*-3-hydroxyvalerate) (PHBV), are ultimately two leaps ahead of other biopolymers as alternatives to petroleum-based polymers.[7,8] However, several challenges exist in producing PHA, including high production cost, energy consumption, and use of non-green toxic chemicals for extraction and dissolution processes.[4] These challenges affect the upscaling and technological uptake of PHA *en masse*, coupled with the variability of the properties of PHA from different producers. To address the challenge of dissolution, a strong uptrend in demand for new greener solvents as substitutes for halogenated organic solvents such as dichloromethane and chloroform has been reported.[9] These halogenated solvents are efficient in PHA dissolution but are toxic and hazardous to biotic and abiotic ecosystems.[10]

As such, dimethyl carbonate (DMC), acetic acid, ionic liquids (ILs), eutectic solvents, ethyl acetate, butyl acetate, ethyl lactate, switchable solvents, *etc.*[11–13] have been fronted as

[a]*Institute of Sustainability for Chemicals, Energy and Environment (ISCE²), Agency for Science, Technology and Research (A*STAR), 1 Pesek Road, Jurong Island, 627833, Singapore. E-mail: lizb@imre.a-star.edu.sg*
[b]*Institute of Materials Research and Engineering (IMRE), Agency for Science, Technology and Research (A*STAR), 2 Fusionopolis Way, Innovis, 138634, Singapore. E-mail: lohxj@imre.a-star.edu.sg*
[c]*Department of Materials Science and Engineering, National University of Singapore, 9 Engineering Drive 1, 117576, Singapore*
†Electronic supplementary information (ESI) available. See DOI: https://doi.org/10.1039/d3gc00793f
‡These authors contributed equally to this work.

less toxic alternative solvents notwithstanding their low dissolution power, high-temperature requirements, and low benefit–cost ratio (BCR). For instance, Zhang and Cran dissolved only 0.5% PHBV in glacial acetic acid (98–99%) at 110 °C.[14] Other studies have reported that acetic acid is not the ideal solvent for PHB dissolution in terms of compatibility.[15] Other interesting solvents are ionic liquids (ILs), with some ILs having exceptional properties such as non-toxicity, high dissolution power, low VOC (volatile organic compounds), and vapor pressure combined with high thermal stability. For instance, Sequeira *et al.* synthesized various ammonium-based ILs and employed them in PHB dissolution.[16] The authors reported maximum solubility of 3% PHB at 70 °C using diethanol ammonium acetate. Compared to chloroform as the gold standard, whose PHB solubility is more than 3-fold at 60 °C, the reported maximum solubility of ILs is considered low. Interestingly, the recovered IL with a high nitrogen content was applied as a biostimulant for liquid fertilizers. In another work, Dubey *et al.*[17] extracted PHB from the bacterial biomass of *Halomonas hydrothermalis* using 1-ethyl-3-methylimidazolium diethyl phosphate and prepared a bioplastic film by solvent casting of the recovered PHB using chloroform. Although IL approaches have been considered green and sustainable, they are not as green as construed because of the complexities in their synthesis and biodegradability challenges.[18] In line with green chemistry principles and sustainability requirements, the search for 'truly' green solvents for the dissolution of biopolymers such as PHAs is essential.[19] To provide such green dissolution media, Abbott *et al.*[20] discovered deep eutectic solvents (DESs) in 2003 and their applications have grown by leaps and bounds in about two decades.[21] A DES is a eutectic mixture of a hydrogen-bond donor (HBD) and a quaternary ammonium or phosphonium salt resulting in a liquid with a melting point below that of its individual components. The individual components of DESs are usually non-toxic and biodegradable compounds making them suitable for green solvent formulation.[22] In the green solvent technology landscape, solvents are evaluated in terms of application conditions such as time, temperature, and concentration; therefore, mild conditions are preferable.[23] Notably, low toxicity DESs such as natural DESs (NADESs), *e.g.* polyphenol eutectic mixtures discovered by Verpoorte *et al.*, have found applications as biosolvents in extraction, dissolution, polymer synthesis, biocatalysis, and biomedicine.[24,25] For instance, D-limonene extracted from essential oils (EOs) has been employed as a suitable biosolvent to extract bioactive compounds to replace oil-based solvents.[26] On the other hand, natural terpenes have been reported as plasticizers for biopolyesters such as PHB.[27] In this regard, naturally derived liquids below 100 °C could be applied as biosolvents for the dissolution of biopolyesters.

Carvacrol (5-isopropyl-2-methylphenol) – an isomer of thymol – is a good example of a model biochemical platform with unique attributes for application as a biobased solvent.[28] Additionally, carvacrol, being hydrophobic with a free hydroxyl group and a phenol moiety, boasts higher antimicrobial activity compared to other volatile compounds or essential oils.[29] These properties limit the widespread industrial application of carvacrol except in oil-in-water (O/W) emulsions or nanoemulsions through an encapsulation technique.[30] The encapsulated oils are dispersible in water and are easily applied in food and beverage industries.[31] On the other hand, carvacrol has found applications in agri-food industries such as animal feed and bactericide production.[32] Because carvacrol is highly preferred for hydrophobic phases, it could be a green solvent for hydrophobic biopolyesters such as PHBV to replace halogenated solvents.[33] The resultant polymer solutions with a high solid content could find applications in functional adhesives and coating formulations due to their intrinsic stickiness.

In this work, we report the solubility performance, rheology, and thermal, chemical, and structural integrity of carvacrol/PHB solutions and regenerated PHB, as well as theoretical predictions of the polymer–solvent interactions using atomistic molecular dynamics (MD) simulations using GROMACS software. To show the potential applicability of the high PHB content in biosolvents as a base material for adhesives, prototype pressure-sensitive adhesive (PSA) was formulated with other biobased additives. Performance such as rheology for viscosity measurements as well as FTIR and NMR for chemical studies was evaluated. WAXD was employed to ascertain changes in the regenerated PHB's structural properties. After regeneration using isopropyl alcohol, the carvacrol biosolvent was recovered in a closed-loop process and characterized by $^1$H NMR. The prototype contact adhesive was characterized using the Dahlquist rheological criterion for tack. Herein, we report the rapid dissolution of high viscosity 20 wt% PHB in carvacrol in a record 30 min at 100 °C not reported or studied so far. Moreover, 1 wt% PHB dissolve even faster within 10 min. Such exceptional conditions of PHB dissolution in a sustainable green medium, which also is intrinsically antibacterial and antioxidant, open potential avenues for PHA applications in coatings, adhesives and packaging with high throughput, short processing time and quality products.

# Experimental

### Chemical reagents and materials

Carvacrol (purity >98%) was purchased from Sigma-Aldrich. Commercial grade poly(3-hydroxybutyrate) (P3HB) ENMAT™ Y3000 (powder form) was purchased from Tianan Biopolymer (China). Gum rosin (GR, softening point of 76 °C and acid number 167) and beeswax were supplied by Sigma-Aldrich. Isopropyl alcohol (IPA) was supplied by Fisher Scientific. All chemicals were used as received.

### Preparation and dissolution of PHB samples in carvacrol

The dissolution of PHB in carvacrol was carried out by heating a known weight of PHB in predetermined amounts of carvacrol solvent, as shown in Table 1. The samples were serialized (A1–A5) and the sample ID was coded as Carv–PHB*x*, where *x* is the concentration of PHB in carvacrol.

Table 1 Carvacrol/PHB samples and conditions for dissolution at 100 °C

| Biopolymer/solvent | Sample ID | Carvacrol wt% | PHB wt% |
|---|---|---|---|
| Carvacrol/PHB | Carv–PHB1 | 99 | 1 |
| | Carv–PHB3 | 97 | 3 |
| | Carv–PHB5 | 95 | 5 |
| | Carv–PHB10 | 90 | 10 |
| | Carv–PHB20 | 80 | 20 |

Fresh carvacrol/PHB samples were placed in 20 mL glass scintillation vials at room temperature and then gradually heated to 100 °C with stirring until an amber to clear homogeneous solution was obtained. The dissolution time method was employed by visualizing the elapsed time for each dissolved sample using a stopwatch by manual timing. The dissolution time was roughly estimated from when the PHB powder was dissolved entirely in carvacrol and formed a transparent amber solution. On the other hand, a visual inspection–optical technique was also employed using an Olympus BX53M optical microscope to observe the Carv–PHB*x* aliquots. The Carv–PHB*x* aliquots were placed between a microscope slide and a cover glass slide forming a circular layer between the glasses. The polymer solution layer was observed perpendicularly to the cover glass, and digital images were captured using a digital camera.

Additionally, PHB was regenerated from Carv–PHB*x* aliquots using isopropyl alcohol (IPA) to obtain PHB particles, and the carvacrol/IPA mixture was recovered by decanting in a closed-loop process. Because of the significant difference in boiling points of IPA and carvacrol, after regeneration of PHB the spent IPA phase (bp: 82.5 °C) was evaporated from the mixture with carvacrol (bp: 236.8 °C) in a rotary vacuum evaporator. The obtained separate phases of IPA and carvacrol could be reused in another cycle thus closing the loop in PHB processing and applications. Both pure carvacrol and recovered carvacrol were characterized using NMR and WAXD to ascertain the purity of the recovered carvacrol.

### Rheological properties

The rheological properties of the carvacrol/PHB solutions at different concentrations were measured using a TA Instruments DHR3 rheometer with a 40 mm circular plate geometry. Temperature gradient tests were performed at a constant shear rate of 4 Hz in the range of 20–100 °C with a temperature ramp rate of 5 °C $min^{-1}$. On the other hand, steady-state flow rheological measurements were performed at constant room temperature (*ca.* 25 °C) in the shear rate range of 0.1–100 $s^{-1}$. Furthermore, to test the applicability of the Carv–PHB20 and Carv–PHB_Adh as potential adhesives, room temperature rheological properties of the samples at 2% strain and 0.01, 0.1, and 1.0 Hz frequencies were analyzed and fitted to the Dahlquist rheological criterion for tack.

### Thermal properties

The thermal properties of the pristine PHB and the regenerated PHB were analyzed by thermogravimetric analysis (TGA) and differential scanning calorimetry (DSC). For TGA analysis, TA Instruments Q500 equipment was used. Samples of about 10 mg were heated in a clean alumina cup from 25 to 600 °C at a heating rate of 20 °C $min^{-1}$ and under ambient atmosphere. The temperature at onset was determined at 5% weight loss ($T_{onset}$) and the temperature at maximal decomposition rate ($T_d$) was determined as the temperature at the main peak of the derivative weight loss curve. Differential scanning calorimetry (DSC) measurements were performed using a DSC instrument (TA Instruments Q100) under a nitrogen atmosphere. The samples were equilibrated at 25 °C, then heated from 25 to 200 °C, cooled to −80 °C, and reheated to 200 °C using a ramping rate of 20 °C $min^{-1}$. Second-run heating cycles were conducted and further used to investigate the phase transition behavior of all samples. Glass transition temperature ($T_g$) was obtained from the midpoint of the slope due to a change in heat capacity, and melting temperature ($T_m$) and crystallization temperature ($T_c$) were obtained from the enthalpy peaks along the curve. We calculated the melting enthalpy as well as heat of crystallization for pristine PHB and regenerated PHB to calculate the crystallinity.

The crystallinity index ($\chi_{DSC}$) was estimated as shown in eqn (1)

$$\chi_{DSC}\,(x\%) = \frac{\Delta H_m}{\Delta H_m^\circ \times w_i} \times 100 \quad (1)$$

where $\Delta H_m$ is the PHB melting enthalpy in the sample, $\Delta H_m^\circ$ is the melting enthalpy for 100% crystalline PHB ($\Delta H_m^\circ = 146\ J\ g^{-1}$) and $w_i = 1.0$ is the weight fraction of the regenerated PHB under test.

**Fourier transform infrared (FTIR) spectroscopy.** The functional groups were determined by FTIR spectroscopy (Bruker Vertex 80V). The FTIR spectra were recorded at a resolution of 2 $cm^{-1}$ and 64 scans, in the range of 4000 to 400 $cm^{-1}$.

**Nuclear magnetic resonance (NMR) spectroscopy.** Nuclear magnetic resonance ($^1$H NMR) spectroscopy was performed using a Bruker 400 MHz spectrometer using $CDCl_3$ as a solvent and internal standard ($\delta$ = 7.26 ppm) at room temperature to characterize the chemical structures of carvacrol and recovered carvacrol.

**Gel permeation chromatography (GPC).** The molecular weight of commercial PHB Y3000 was obtained using an Alliance Waters 2695 GPC equipped with an Alliance Waters 2414 refractive index detector. HPLC-grade chloroform was used as the eluent at a flow rate of 1.0 mL $min^{-1}$ at 40 °C. A set of polystyrene standards with a molecular weight range from 500 to 7 × $10^6$ Da was used to calibrate the gel permeation chromatography equipment and analyses were carried out using Empower 3 software. The number-average ($M_n$) and weight-average molecular weight ($M_w$) of commercial PHB were estimated.

**Wide angle X-ray diffraction (WAXD) analysis.** To gain insights into the crystallographic structure of PHB after dissolution and regeneration, WAXD patterns were recorded using a Bruker GADDS diffractometer (D8 Discover μMR). The operating voltage was 50 kV for the area detector and a current of

 

800 μA, with Cu Kα radiation ($\lambda$ = 1.5418 Å) at room temperature. The WAXD diffractograms were obtained as a function of $2\theta$ in the range of 5–60°.

### Dissolution mechanism: atomistic molecular dynamics simulation study

In this study, the force field used is the general amber force field (GAFF)[34] which has been successfully used to describe PHB and carvacrol in previous research.[35,36] The initial structures of PHB (containing 20 repeating units) and carvacrol were built using Avogadro software.[37] Four simulation boxes were built with a side length of 10 nm. Each simulation box contained 1146 carvacrol molecules with a varying number of PHB molecules to account for the correct mass fraction: 3 for 0.03, 5 for 0.05, 11 for 0.10, and 25 for 0.20. PHB and carvacrol molecules were randomly packed into the simulation box using Packmol[38] software for the four different systems. All the systems were first energy minimized and then equilibrated in the constant temperature, constant volume (*NVT*) ensemble at a temperature of 293.15 K for 1 ns and 20 ns in the constant temperature, constant pressure (*NPT*) ensemble (temperature of 293.15 K and pressure of 1 bar). Finally, 20 ns runs were performed in the *NPT* ensemble with a temperature of 373.15 K and a pressure of 1 bar. All the above simulations were performed within the GROMACS[39] software package under periodic boundary conditions. The time step used in the simulation was 1 fs. For long-range electrostatics, the Particle-Mesh Ewald (PME) method was used.

## Results and discussion

### Dissolution of PHB in carvacrol

Due to sustainability concerns, the search for biosolvents for application in the processing of biopolyesters has grown tremendously over the years.[9] In these endeavors, phenolic compounds from plants have been successfully used in the preparation of natural deep eutectic solvents (NADESs) and in the synthesis of biobased adhesives.[40] However, deep eutectic solvent mixtures are composed of at least two components. Herein, we employ one component consisting of a plant-derived biosolvent called carvacrol to dissolve the bioplastic PHB. Interestingly, carvacrol biosolvent rapidly dissolved PHB of different concentrations ranging from 1 to 20 wt%. As seen in Fig. 1A, Carv–PHB20 completely dissolves within half an hour, whereas Carv–PHB1 dissolves in a record 10 min. The other intermediate samples dissolved within the timeline of 10–30 min. This can be ascribed to the small molecule of carvacrol diffusing into the PHB structure and rapidly disrupting the intermolecular bonding, thus disintegrating the biopolymer.[41] It has been reported that the dissolution of polymers occurs in 2 stages of transport processes, *i.e.*, solvent diffusion and chain disentanglement. There are many techniques that have been reported to study polymer dissolution such as differential refractometry, optical microscopy, interferometry, ellipsometry, steady-state fluorescence, nuclear magnetic resonance (NMR) and FT-IR imaging, but all these methods do not have real-time measurements to indicate the time taken for complete dissolution of the polymers.[42] The dis-

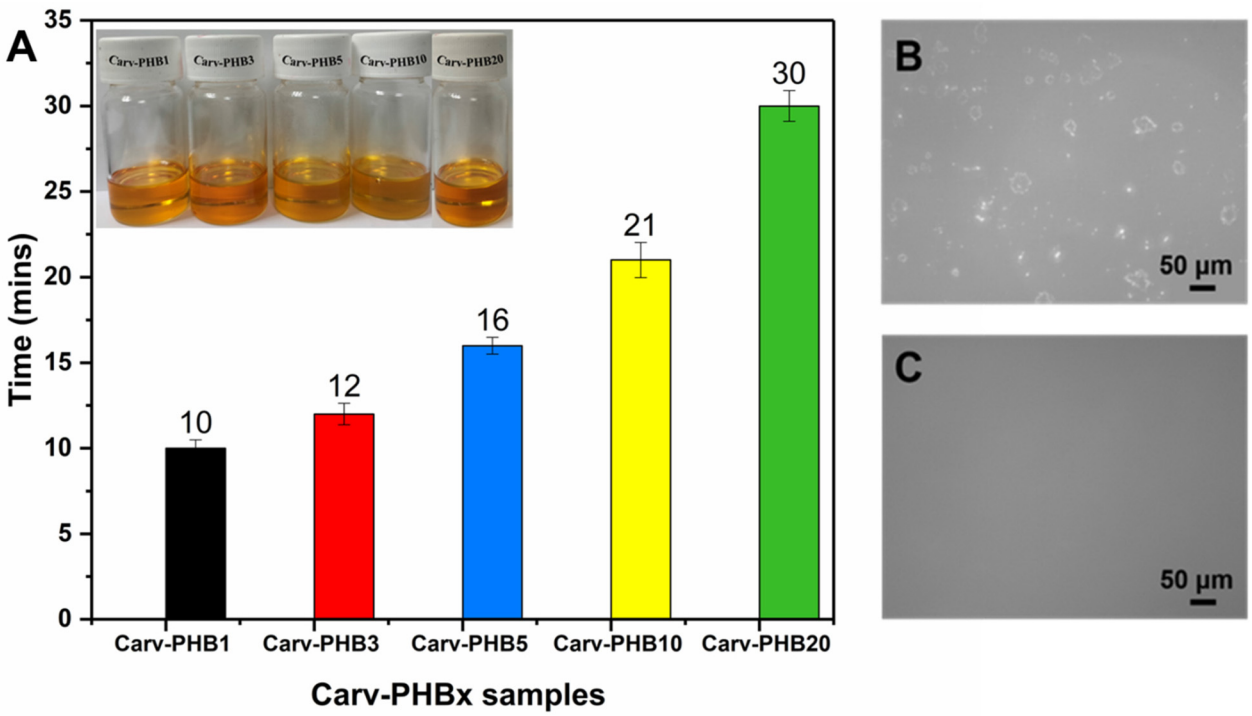


**Fig. 1** (A) Dissolution times of PHB using a biosolvent (carvacrol) with the inset showing pictures of solutions labelled 1, 3, 5, 10 and 20 wt%; (B) Carv–PHB20 sample before dissolution and (C) after complete dissolution.

solution clock approach discovered by Peppas *et al.*[43] remains the preferred method to estimate the time taken for dissolution. In this approach, the clock is initially set to zero and after a period equal to the reptation time, the polymer dissolves. Although this method is subjective, the obtained solution can be ascertained whether it is fully dissolved using other techniques. Repeated cycles of dissolution by the clock method help to obtain the average time of dissolution of the polymer at different concentrations and we have included error bars to allow for deviations from the average time. It is worth noting that the solutions exhibited stability with no apparent signs of visible residues even for the highly concentrated Carv–PHB20 sample shown in Fig. 1(B and C) after dissolution. To qualitatively ascertain PHB dissolution, visual and optical observations were made on selected samples before and after dissolution. As shown in Fig. 1C, no residues were observed for the Carv–PHB20 sample after dissolution compared to the visible residues on the glass plates before dissolution (Fig. 1B). The results confirm that carvacrol is potentially a suitable solvent for biopolyesters, especially PHAs. Moreover, the rapid dissolution in polymer processing undoubtedly increases productivity and throughput and leads to improved profits. It is worth noting that carvacrol has also been reported to possess antibacterial and antifungal properties, which would be useful in producing PHB-based antibacterial adhesives and green coatings.[32] To compare the properties and capabilities of green solvents, we have summarized selected green solvents used in the PHB processing value chain. This work shows the comparative advantages over other green solvents as depicted in Table 2. This is because comparatively the commercial PHB (Y3000) had number average ($M_n$ = 1.62 × $10^5$ Da), GPC and weight average ($M_w$ = 2.06 × $10^5$ Da) molecular weights and PDI ($M_w/M_n$: ~1.28) as determined using GPC.

### Thermal properties of pristine PHB and the regenerated PHB

The thermal properties of the PHB samples were determined by TGA and DSC. Fig. 2A shows the DSC curve of the pristine PHB and the regenerated PHB during the first cooling and second heating cycles. As seen in Fig. 2A, the crystallization temperatures during the cooling cycle are similar for both the pristine PHB and the regenerated PHB. The regenerated PHB exhibited a sharper peak denoting faster crystallization ability. This phenomenon could be ascribed to complex interactions with PHB resulting in the enhancement of cold crystallization ($T_{cc}$) compared with pristine PHB. This complex interaction is manifested by the pronounced cold crystallization peak of regenerated PHB compared with pristine PHB which appears somehow flat and broadened. Carvacrol has been reported to serve many roles such as a plasticizer, nucleator, *etc.*[49,50] During the heating process, both PHBs exhibited relatively similar

**Table 2** Selected green solvents in the PHA value chain in processing and applications

| Green solvent | Features | Source | Dissolved polymer molecular weight and method | Conditions | Dissolution capacity | Value chain | Ref. |
|---|---|---|---|---|---|---|---|
| Acetic acid | Corrosive | By-product of fermentation | 1.9 × $10^5$ Da; GPC | Boiling, 40–60 min | 5% w/v | Application | Elias *et al.*[15] |
| Ammonium-based ionic liquids (ILs) | Non-toxic and non-corrosive | Synthesis | 1.71 × $10^5$ Da; Ostwald viscometer | 70 °C | 3% w/v | Application | Sequeira *et al.*[16] |
| 1,3-Dioxolane | Non-toxic, non-carcinogenic, and miscible in water | Synthesis | 1.82 × $10^5$ Da (PDI = 4.79); GPC | 100 °C/4 h | 5% (83.9% efficiency) | Extraction (downstream) | Yabueng & Napathorn[44] |
| 2-Methyltetrahydrofuran (2-MTHF) | Non-irritating | Renewable resources (corncobs, bagasse) | 1.82 × $10^5$ Da; GPC | 100 °C/4 h | 2.5% (30% efficiency) | Extraction (downstream) | Yabueng & Napathorn[44] |
| Butyl acetate | Medium toxicity | Synthesis | 1.2 × $10^6$ Da; Ubbelohde dilution viscometer | 100 °C/1 h | 7% (97% efficiency) | Extraction (downstream) | Aramvash *et al.*[45] |
| Dimethyl carbonate | Low toxicity, non-irritating and non-mutagenic | Synthesis | 1 × $10^5$ Da; GPC | 90 °C/1.5 h | 2.5% (69% efficiency) | Extraction (downstream) | Schuur *et al.*[46] and Beatrice *et al.*[47] |
| Ethyl acetate | Low toxicity | Synthesis | 1.2 × $10^6$ Da; Ubbelohde dilution viscometer | 100 °C/1 h | 7% (97% efficiency) | Extraction (downstream) | Aramvash *et al.*[45] and Martinelli *et al.*[48] |
| **Carvacrol** | **Non-toxic, biodegradable, and non-carcinogenic** | **Renewable resources and synthesis** | **$M_n$ = 1.62 × $10^6$ Da, $M_w$ = 2.06 × $10^6$ Da ($M_w/M_n$: ~1.27); GPC** | **100 °C/ 30 min** | **20% w/v** | **Application** | **This work** |

 

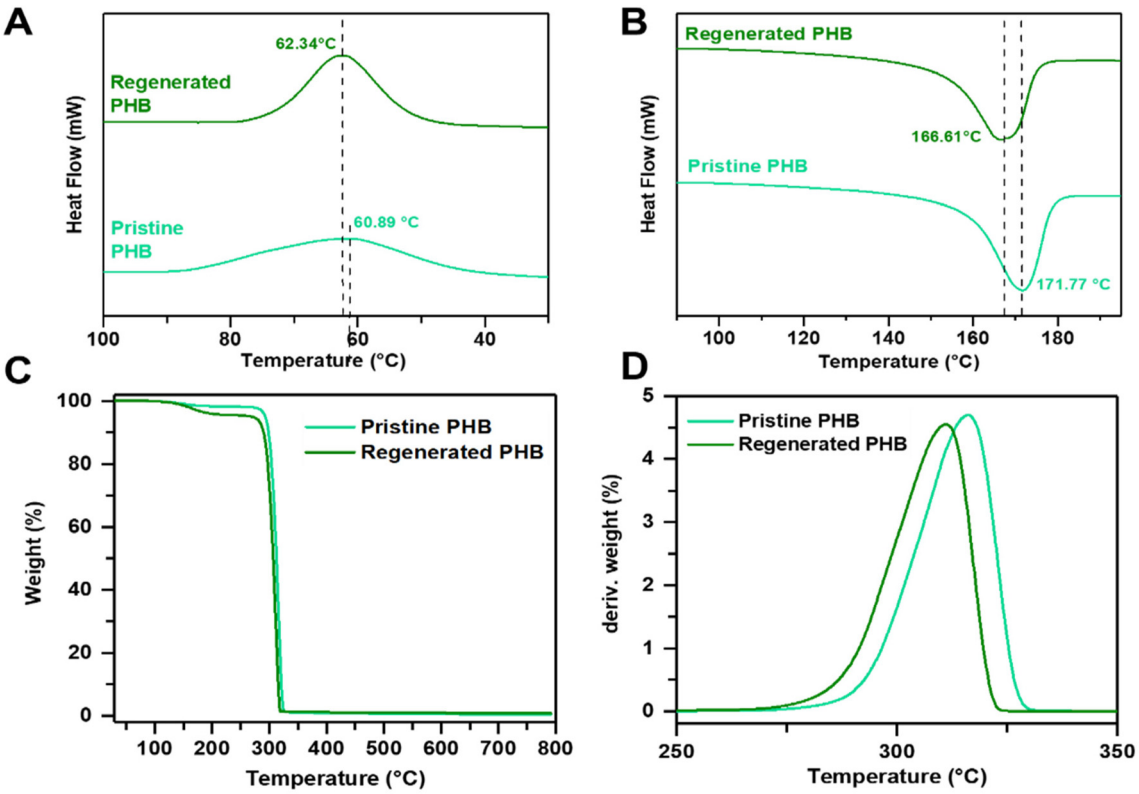


**Fig. 2** DSC (A) first cooling curve and (B) second heating curves and TGA heating curves of (C) weight loss, and (D) derivative weight of pristine PHB and regenerated PHB.

glass transition temperatures ($T_g$) at −2.58 and 0.81 °C, respectively. Similarly, the melting temperatures ($T_m$s) were around 171.77 °C and 166.61 °C, respectively, as shown in Fig. 2B. However, the crystallinity of the pristine PHB was calculated and found to be around 63.1%, slightly higher than that of the regenerated PHB at 55.9%. The depression in the melting behavior is related to the segmental motion of polymer chains, in this case, possibly due to the presence of impurities (or remnant carvacrol) that disrupted the crystallization process.[51] In addition, thermal stability was investigated using TGA, as shown in Fig. 2(C and D). It can be observed that the pristine PHB displayed a single degradation profile with a $T_{onset}$ value of 293.14 °C with 5% mass loss and a decomposition temperature of 316.13 °C. In contrast, the regenerated PHB showed slightly lower thermal stability, with a $T_{onset}$ value of 270.61 °C with 5% mass loss and a decomposition temperature of 311.07 °C. The mass loss is ascribed to the polymeric random β-chain scission of the –C═O and C–O bonds in the ester.[16,51,52]

### FTIR of PHB and regenerated PHB

The FTIR spectra of both the PHB and the regenerated PHB are displayed in Fig. 3, showing great similarities at various peaks. Typically, PHB's functional groups and moieties are –C–O, –C═O, and –CH.

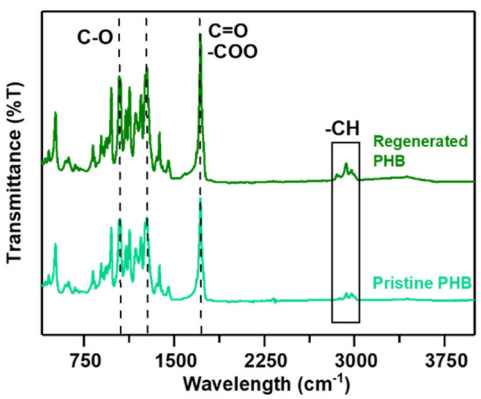


**Fig. 3** Fourier transform infrared (FTIR) spectra of pristine PHB and regenerated PHB in IPA.

As can be seen, the characteristic band observed at 1054 to 1289 $cm^{-1}$ corresponds to the C–O bonding, while the band observed at 1727 to 1734 $cm^{-1}$ corresponds to the strong $\nu$(C═O) (carbonyl) and –COO (ester) groups. The band at 2930 to 2975 $cm^{-1}$ represents the presence of –CH (alkane) bonding, which is in good agreement with the literature.[16,52] In terms of peaks, the bands of the regenerated PHB samples show significant similarity with and a substantial degree of purity to those of the pristine PHB.

### Wide angle X-ray diffraction (WAXD) analysis

Because PHB is biogenic, its configuration is near perfect, with very high crystallinity arising from only one optically active form.[53] Typically, the $3_1$ helix α-form of PHB crystals with a 2-fold screw axis is dominant but the zigzag conformed β-form crystals also do coexist.[27] Fig. 4(A and B) show 2D images and X-ray diffraction peaks of both the pristine PHB and the regenerated PHB, respectively. These WAXD patterns of the regenerated PHB in IPA can ascertain the retention of the original PHB structural integrity.

As can be seen, the WAXD diffractogram of the pristine PHB in the $2\theta$ range 5–55° shows seven prominent peaks at $2\theta$ = 13.5, 16.9, 22.5, 25.5, 27.3, 30.2 and 36.7°, corresponding to the Miller indices of the (020), (110), (111), (121), (040), (002) and (122) planes.[27] Other much smaller peaks are observed at $2\theta$ values of 40.7°, 44.2°, and 49° representing the (151), (222), and (103) indices.[54] However, there exist small amounts of β-form crystals at around $2\theta$ = 20.1° which agrees with earlier studies on PHB crystallography and other studies have reported a peak between $2\theta$ = 10–12° like our pristine PHB.[55,56] Although the regenerated PHB in IPA only depicts a shoulder at $2\theta$ = 15° compared to a noticeable peak for the pristine PHB, other peaks remain practically unchanged for the regenerated PHB in IPA (Fig. 4B). This observation suggests that the structural information of the pristine PHB is not appreciably lost through regeneration.

The choice of IPA as a non-solvent was crucial for the ease of recovery of the carvacrol biosolvent through distillation after separating the precipitate with a yield of 94%. To further characterize the regenerated PHB's purity, proton NMR was conducted, as shown in Fig. 5. The regenerated PHB presents the characteristic signals of the backbone containing (–CH), which has a resonance at 2.5 ppm (labeled red as b) and 5.3 ppm (labeled red as c), while the methyl group ($-CH_3$) has a resonance at 1.3 ppm (labeled red as d). These peaks are similar to those of the reference purified PHB. Notably, the regenerated PHB exhibits characteristic signals similar to those of carvacrol attributed to the residual trace of carvacrol. The peaks associated with the methyl protons (–CH) of the cyclic compound of carvacrol were identified at 6.8 ppm (labeled blue as peaks a and d) and 7.1 ppm (labeled blue as peak e). The methyl proton (–CH) of the aliphatic chain was identified at 2.8 ppm (peak b) together with the three methyl end groups ($-CH_3$) at 1.2 ppm (labeled blue as peak c) and 2.2 ppm (labeled blue as peak f). In comparison, the pristine PHB (Y3000), a commercially available PHB, has characteristic signals of PHB and other signals at the resonance of 3.6 ppm and 4.4 ppm that correspond to the additives. It is worth noting that the regenerated PHB does not contain the additives as the extra peaks are not present, further showing the possibility of the dissolution of PHB in carvacrol as a green solvent and the removal of impurities for further downstream processes.

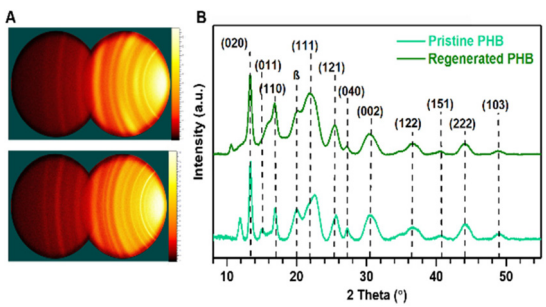


Fig. 4 (A) GADDS images corresponding to (B) WAXD plots of intensity *versus* $2\theta$ for the pristine PHB and the regenerated PHB in IPA.

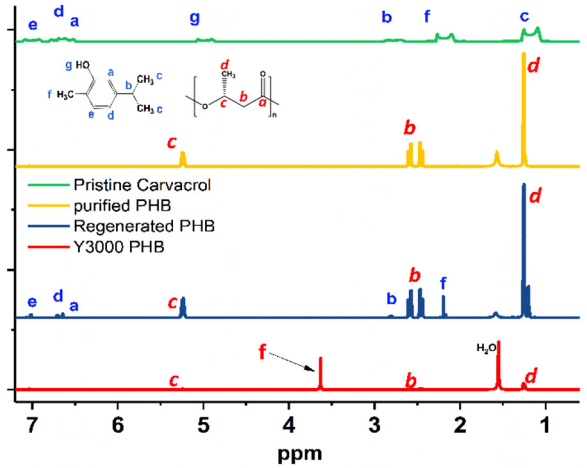


Fig. 5 $^1$H NMR spectra of pristine PHB (Y3000), regenerated PHB, purified PHB (as reference) and pristine carvacrol in $CDCl_3$.

Through the distillation method, the carvacrol biosolvent and IPA can be recovered and reused in similar regeneration cycles. Furthermore, the chemical structure of the recovered carvacrol biosolvent is like the pristine carvacrol, as seen in $^1$H NMR analysis in Fig. S1 (ESI†), albeit a slightly deep color is observed by visual inspection. As observed in Fig. S1,† the peaks associated with the methyl protons (–CH) of the cyclic compound of carvacrol were identified at $\delta$ = 6.8 (peaks a and d) and 7.1 ppm (peak e). The methyl proton (–CH) of the aliphatic chain was identified at 2.8 ppm (peak b) together with the two methyl end groups ($-CH_3$) at 1.2 ppm (peak c) and 2.2 ppm (peak f), similar to the reported literature.[57] Clearly, the recovered carvacrol has a highly resembling peak of the pristine carvacrol, demonstrating success in the solvent recovery process. More importantly, this dissolution and regeneration of the PHB process could also suggest the applicability of the carvacrol biosolvent in the biorefinery processing of PHAs, thus replacing toxic halogenated chemicals.

### Rheological properties

The flow or non-flow of polymer systems denotes the viscosity values of materials. The rheological studies of such systems provide insights into the viscoelastic properties of materials. These properties are particularly important in liquid polymer systems such as adhesives, sealants, and coatings in terms of

 

temperature dependence and the shear rate during formulation and application.[58] In this regard, temperature-dependent viscosity tests were performed on selected carvacrol/PHB samples from 25 °C to 100 °C within 15 min (5 °C $min^{-1}$). On the other hand, the viscosity of the selected carvacrol/PHB solutions was determined at a constant temperature (25 °C) and at varying shear rates between 0.1 $s^{-1}$ and 100 $s^{-1}$. Under varied temperature viscosity measurements, all the samples markedly depict the Arrhenius consistent viscosity decrease with temperature, as shown in Fig. 6A, with samples Carv–PHB3 and Carv–PHB5. However, Carv–PHB20 shows viscosity perturbations at a low temperature (20–40 °C), but above this point the viscosity decreases smoothly with a temperature increase.

Apparently, this is ascribed to the loss of cohesiveness because of the decrease in the activation energy barrier as temperature weakens the major attractive forces and enhances the mobility of the molecular chains in the polymer system. Additionally, the decreased energy needed for the flow leads to a decrease in the interference of the hydrodynamic domains, reduced inter-chain liaisons and increased polymer solubility.[59]

Furthermore, a decrease in the viscosity of the selected carvacrol/PHB samples with temperature, and the activation energy barrier dependence on temperature can be described by the Arrhenius law and computed by a plot of logarithmic viscosity *versus* reciprocal absolute temperature as shown in eqn (2).

$$\eta = \eta_{\infty}\, e^{(-E_a/RT)} \quad (2)$$

where $\eta$ is the viscosity in mPa s, $\eta_{\infty}$ is the zero-shear viscosity in mPa s, $E_a$ is the activation energy of flow in kJ $mol^{-1}$, $R$ is the ideal gas constant in kJ $mol^{-1}$ $K^{-1}$, and $T$ is the temperature in Kelvin (K). In plotting the $\ln \eta$ against $T^{-1}$ ($K^{-1}$), the activation energy barriers of the samples can be obtained as the slope of the graph. Fig. 6B depicts the logarithmic plots of viscosity and reciprocal temperature in Kelvin. In all the cases, the activation energy barrier increases with concentration as depicted by the gradients of the graphs in Fig. 6B, and calculated to be 35.63, 35.82, 36.58, and 27.26 kJ $mol^{-1}$ for Carv–PHB3, Carv–PHB5, Carv–PHB10 and Carv–PHB20, respectively, as in Table S1.† These activation energies closely agree with previously reported figures of 37–40 kJ $mol^{-1}$ for pure PHB.[60] The observed high activation energy barrier for samples Carv–PHB3, Carv–PHB5, and Carv–PHB10 show that viscosity is highly temperature-sensitive with the stronger polymer chain interactions in the solvent and correspondingly more restricted chain mobility. Moreover, thermal motion of the molecules is a primary factor affecting the viscosity–temperature relationship for low concentration samples.[60]

Typically, for the viscous flow of polymer solution, the activation energy monotonically increases with an increase in polymer concentration. Contrarily, the more viscous Carv–PHB20 sample depicts a sudden reduction in the activation energy barrier ($E_a$), which suggests a change in molecular associations such as hydrogen bonding, or physical crosslinks of π–π interactions and the limiting viscosity number is highly temperature dependent.[61] More importantly, molecular interaction dynamics (described in detail in the Dissolution mechanism section) offer an opportunity to decipher these changes in molecular associations.[62] Furthermore, shear dependence on viscosity is important as it may affect the material's processability and applicability. This is because shearing forces induce microstructural rearrangements in polymer solutions, gels, or suspensions. In this regard, Fig. 7 shows the rheological profiles (viscosity *vs.* shear rate) of Carv–PHB*x* samples at room temperature.

As can be seen in Fig. 7, low concentration samples (Carv–PHB3, Carv–PHB5) depict a near Newtonian behavior at low and high frequencies and the viscosity is nearly independent

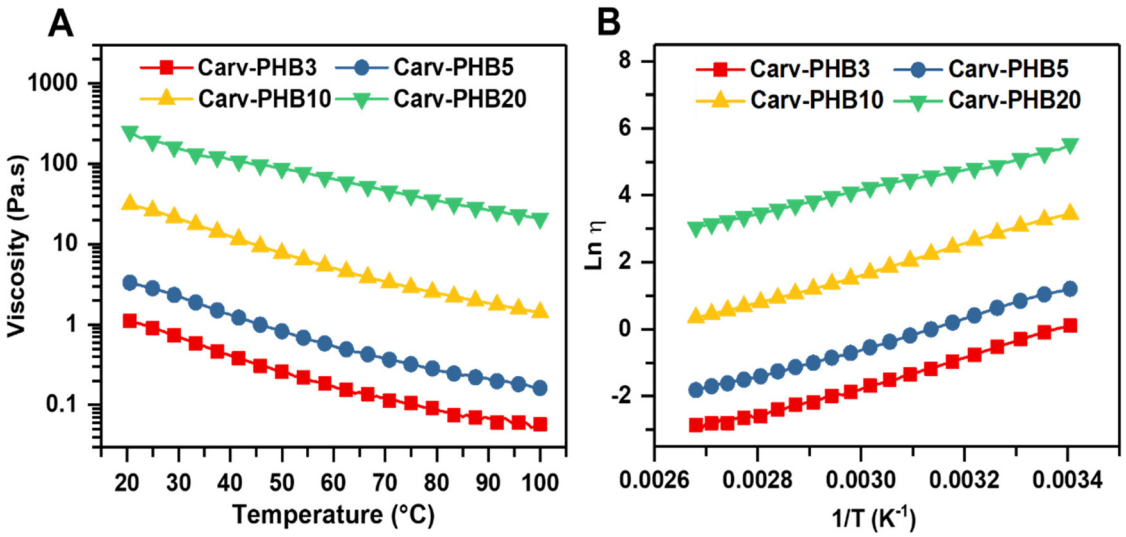


**Fig. 6** (A) Temperature effects on viscosity and (B) $\ln \eta$ plotted against inverse temperature $1/T$ ($K^{-1}$) for selected Carv–PHB*x* samples.

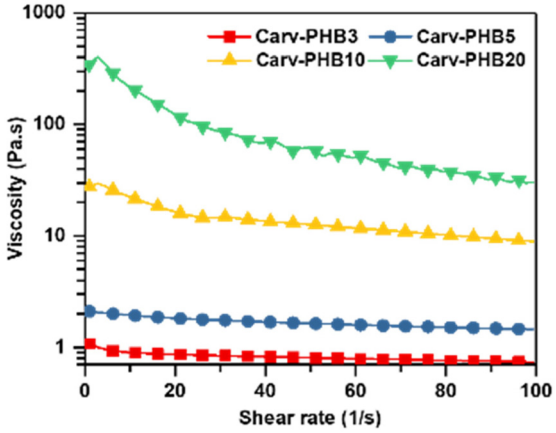


**Fig. 7** Rheological profiles (viscosity–shear rate) for selected Carv–PHB*x* samples.

of the frequency. This characteristic is ascribed to the near non-existent interactive structure of the polymer solutions and is exacerbated by the low concentration of the polymer chains in the solvent. Contrarily, Carv–PHB10 and Carv–PHB20, which are higher concentration PHB samples, display shear thinning characteristics. These samples have high viscosity in the low shear region (non-Newtonian behavior) and shear thinning characteristics towards the mid and high shear regions. This 'double life' viscosity behavior of the polymer systems is interesting because it dictates the handling of formulated products such as adhesives or coatings from blending, pumping, and storage. In addition, molecular movements and the flow behavior of a polymer system are better understood by comparing the storage modulus ($G'$) and loss modulus ($G''$) plots against temperature. $G'$ is equal to $G''$ are inversely proportional to temperature with no crossover point for samples Carv–PHB3, Carv–PHB5, and Carv–PHB10 (Fig. S2†). This behavior indicates the non-existence of solid/liquid or liquid/solid transition, which is usually marked ($x$) by the crossover modulus and crossover temperature (Fig. S2†). This phenomenon is probably due to the low polymer concentration; therefore, the solution is in liquid form even at room temperature. However, a crossover temperature of about 28 °C exists for the Carv–PHB20 sample and a corresponding crossover modulus of about 1.326 kPa. Below the crossover point, $G'$ slightly dominates $G''$ which indicates a solid-like behavior due to the likely presence of physical crosslinks. Conversely, above the crossover point, $G''$ significantly dominates over $G'$ which clearly denotes the liquid-like behavior due to permanent deformation of the liquid polymer solution.

### Potential application: PHB–carvacrol renewable bioadhesive

A polymer solution qualifies as sticky or tacky if under very light pressure it possesses the ability to adhere instantaneously to a solid surface.[63] Qualitatively, the stickiness or tackiness of a formulated solution can be evaluated by placing it between two solids and analyzing its resistance which must be overcome to separate the jointed solids.[64] In this regard, the observed tackiness of Carv–PHB20 suggests that it has potential as a base formulation for bioadhesive applications, albeit it needs additives (tackifiers, waxes, plasticizers) to improve the adhesive properties and performance. In this work, we analyzed the rheological properties of the Carv–PHB20 sample as a base formula for adhesives because of its high enough concentration of a sticky ingredient. Using the Dahlquist criterion discovered by Carl A. Dahlquist, we studied the rheological control and mechanism of Carv–PHB20 and the additive-modified Carv–PHB20 (denoted as Carv–PHB_Adh) as a prototype bioadhesive (composition shown in Table S2†).

Dahlquist, in his rheological criterion for tackiness/stickiness, unearthed that tackiness does not occur when the storage modulus of the adhesive formulation is greater than $3 \times 10^5$ Pa at a frequency of 1 Hz for wetting the surface instantaneously.[65] This criterion helps induce and gain initial insights into the relationship between the tackiness and linear viscoelasticity properties of the selected Carv–PHB20 sample and Carv–PHB_Adh. Fig. 8 shows the frequency dependency of shear modulus ($G'$, $G''$) for Carv–PHB20 and Carv–PHB_Adh, respectively. As can be seen, Carv–PHB20 possesses adhesive properties but has too low $G'$ compared to the Dahlquist requirement ($G' \leq 3 \times 10^5$ Pa) at the bonding frequency (1 Hz) and therefore can only be applied as a standard adhesive as it lacks shear resistance (low cohesive strength).[66]

However, Carv–PHB20 could be enhanced with additives such as tackifiers (gum rosin, natural beeswax, *etc.*) to obtain a higher $G'$ at 1 Hz to meet the Dahlquist criterion. As seen in Fig. 8, Carv–PHB_Adh possesses a $G'$ value of about $2 \times 10^5$ Pa at a bonding frequency of 1 Hz and therefore sufficiently meets the Dahlquist criterion for high tack adhesive applications.

On the other hand, the $G''$ value of about $1 \times 10^5$ Pa for Carv–PHB_Adh at the same frequency (1 Hz) is still within the Dahlquist criterion range, and this supports the concept of potential application as removable pressure sensitive adhesive and could be positioned in the type 2/central region of Chang's viscoelastic window.[58] Notably, the maximum tack

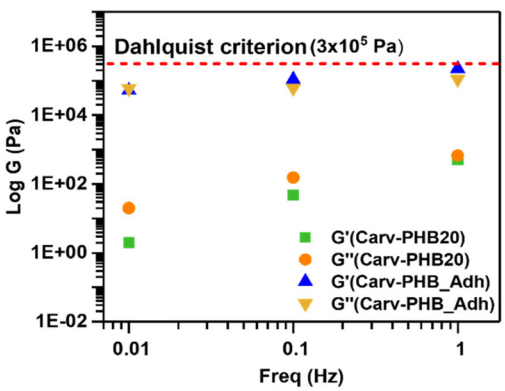


**Fig. 8** Storage and loss modulus *vs.* frequency plot for Carv–PHB20 and Carv–PHB_Adh.

energy is obtained from the maximum tan $\delta$ ($G''/G'$), which corresponds to a higher viscous flow.[67] Deplace, F., *et al.* noted that the value of tan $\delta/G' > 5$ MPa$^{-1}$ is ideal for high surface energy materials (*e.g.*, steel).[68] In this regard, the tan $\delta/G'$ value of the Carv–PHB_Adh bioadhesive at a bonding frequency of 1 Hz is about 1 MPa$^{-1}$, probably because of the lack of extensive entanglements and will likely fail due to interfacial cracks.[69]

### Dissolution mechanism: molecular interaction analysis

Although experiments can provide real-time data on the solubility of polymers and other interactions, atomistic molecular dynamics (MD) simulations complement tests on the laboratory bench as a modern tool for efficient and cost-effective processes. MD simulations not only provide theoretical data but also supply detailed information relating to the strength and interactions at the atomic level. To understand the interactions, especially the remarkable decrease in activation energy for the highly viscous Carv–PHB20 solution, we employed GROMACS software in our work. By employing atomistic simulations, the change in the total hydrogen bonds, and bond formation and breaking for polymer–solvent, solvent–solvent, and polymer–polymer interactions could be decrypted.

In this study, the force field used is the general amber force field (GAFF)[34] which has been successfully used to describe PHB and carvacrol in previous research.[35,36] The initial structures of PHB (containing 20 repeating units) and carvacrol were built using Avogadro software[37] and the dissolution mechanism MD simulation study followed was as described in the Methods section. Fig. 9 depicts snapshots of equilibrated simulation cells containing PHB/carvacrol molecules at different concentrations of (A) 3%, (B) 5%, (C) 10% and (D) 20%, and the detailed simulation data are presented in Table S3.†

The snapshots show that at low concentrations (dilute and semi-dilute) the PHB molecules are well surrounded by the carvacrol molecules with possibly greater interactions that lead to the rapid dissolution of PHB. The results suggest that carvacrol molecules diffuse easily into the interior of the PHB molecules to destroy the inter- (C–H···O=C) hydrogen bonds of PHB.[70] It is worth noting that different solvents exhibit diverse mechanisms in the dissolution of polymer chains.

Typically, PHB has a $3_1$-helix configuration and, on dissolution, this helical structure is maintained in solutions, but helix–coil transition is observed by varying the temperature or solvent composition.[71] Therefore, in terms of helix–coil transition theory, the low concentration samples below the overlap concentration ($c^*$) are coiled with the breaking of many hydrogen bonds. This hydrogen bond breaking increases with a concentration of up to 0.1 mass fraction. When the hydrogen bonds break, the chains can assume randomly coiled configurations typical to chain polymers. In this regard, the simulation data (Table S2†) on hydrogen bond analysis show that Carv–Carv H-bonds are dominant compared with PHB–Carv H-bonds for all the samples except Carv–PHB20 at 373.15 K and the diffusion coefficient decreases with concentration. However, at higher concentrations above the overlap concentration ($c^*$), especially Carv–PHB20, the PHB chain segments exist both as helical and coiled in the solvent (carvacrol) and therefore H-bond breaking (~179) is less compared with the

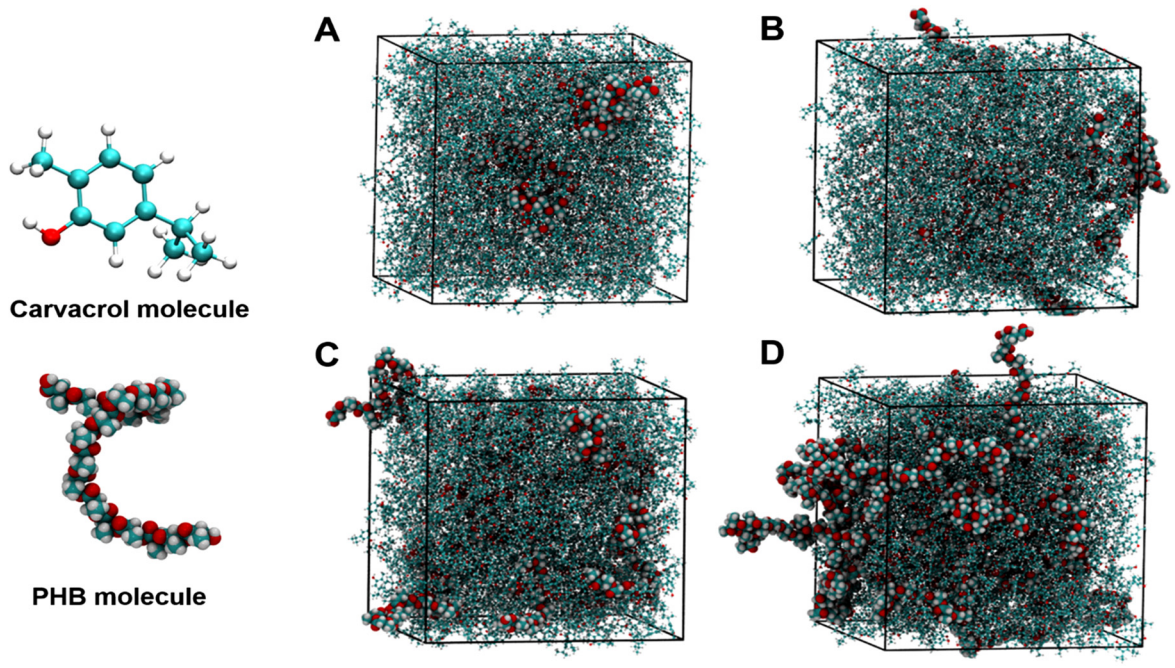


**Fig. 9** Snapshots of equilibrated simulation cells containing PHB/carvacrol molecules at different concentrations of (A) 3%, (B) 5%, (C) 10% and (D) 20%. Red corresponds to O atoms, cyan to C atoms, and white to H atoms.

low concentration samples (202–209). The existence of both helical and randomly coiled chain segments of PHB possibly explains the high viscosity and low diffusion ($3.7 \times 10^4$ cm$^2$ s$^{-1}$) of the sample. Although the activation energy ($E_a$) of the Carv–PHB20 sample (27.3 kJ mol$^{-1}$) is expected to be higher than that of the low concentration samples, the coexistence of helical and randomly coiled PHB segments lowers the activation energy as calculated using the Arrhenius formula reported in the Rheological properties section presented earlier. Moreover, the results suggest that although H-bonding interactions are paramount in the dissolution mechanism of polymers, other parameters do affect the efficiency of dissolution.[72] For instance, carvacrol has been used as a thermal plasticizer and therefore could play the dual role of plasticization and dissolution.[61]

## Conclusions

This work successfully used carvacrol – a natural terpenoid – to rapidly dissolve PHB within 30 min for concentrations of up to 20%. Furthermore, Carv–PHB aliquots were precipitated in isopropyl alcohol (IPA) to regenerate PHB and recover the solvent (carvacrol) for recycling. The pristine PHB and the regenerated PHB were similar as characterized by FTIR and WAXD. On the other hand, the recovered carvacrol from IPA had a similar structure as characterized by $^1$H NMR. Interestingly, the Carv–PHB20 solution was sticky and demonstrated potential for use as a base polymer for bioadhesives. Although rheological studies showed that Carv–PHB20 satisfied the Dahlquist criterion for tack ($G' \leq 3 \times 10^5$ Pa) at the bonding frequency (1 Hz), its $G'$ value ($<3 \times 10^2$ Pa) was too low. After modulation using a tackifier and natural beeswax, the resultant $G'$ was acceptable with a value of $\leq 2 \times 10^5$ Pa. On the other hand, the dissolution mechanism was elucidated by molecular dynamics (MD) simulations using GROMACS software. Interestingly, a high concentration sample (Carv–PHB20) depicted a lower density of hydrogen bond breaking which suggests the existence of both helical and coiled PHB segments in the solvent using helix–coil transition theory. Contrarily, low concentration samples have a high density of hydrogen bond breaking and likely, most of the PHB segments are coiled entrapping the solvent which affects the diffusion coefficient values with an increase in concentration. This work undoubtedly opens the frontier of dissolution of biopolyesters using carvacrol and possibly other monoterpenoids for potential applications in adhesive, coating and sealant industries.

## Author contributions

Joseph Kinyanjui Muiruri: writing – original draft. Jayven Chee Chuan Yeo: writing – original draft. Tang Yuanting Karen: conceptualization, data curation, validation, and visualization. Ke Li: conceptualization, data curation, validation, and visualization. Enyi Ye: conceptualization, project administration, supervision, resources, and writing – review & editing. Xian Jun Loh: conceptualization, project administration, supervision, resources, and writing – review & editing. Zibiao Li: conceptualization, project administration, supervision, resources, and writing – review & editing. All the authors have read and agreed to the published version of the manuscript. Joseph Kinyanjui Muiruri and Jayven Chee Chuan Yeo contributed equally to this work.

## Conflicts of interest

There are no conflicts to declare.

## Acknowledgements

This project was supported by the RIE2025 Manufacturing, Trade and Connectivity (MTC) Programmatic Fund (M22K9b0049) and AME Young Individual Research Grants (YIRG) (Grant No. A2084c0168) administered by A*STAR.

## References

1 V. G. Zuin and K. Kümmerer, Chemistry and materials science for a sustainable circular polymeric economy, *Nat. Rev. Mater.*, 2022, **7**(2), 76–78.
2 C. Gioia, G. Giacobazzi, M. Vannini, G. Totaro, L. Sisti, M. Colonna, P. Marchese and A. Celli, End of life of biodegradable plastics: composting versus Re/upcycling, *ChemSusChem*, 2021, **14**(19), 4167–4175.
3 S. F. Hansen, R. Arvidsson, M. B. Nielsen, O. F. H. Hansen, L. P. W. Clausen, A. Baun and A. Boldrin, Nanotechnology meets circular economy, *Nat. Nanotechnol.*, 2022, 1–4.
4 J. K. Muiruri, J. C. C. Yeo, Q. Zhu, E. Ye, X. J. Loh and Z. Li, Poly(hydroxyalkanoates): Production, Applications and End-of-Life Strategies–Life Cycle Assessment Nexus, *ACS Sustainable Chem. Eng.*, 2022, **10**(11), 3387–3406.
5 Z. Li, J. Yang and X. J. Loh, Polyhydroxyalkanoates: opening doors for a sustainable future, *NPG Asia Mater.*, 2016, **8**(4), e265.
6 J. C. C. Yeo, J. K. Muiruri, B. H. Tan, W. Thitsartarn, J. Kong, X. Zhang, Z. Li and C. He, Biodegradable PHB-rubber copolymer toughened PLA green composites with ultrahigh extensibility, *ACS Sustainable Chem. Eng.*, 2018, **6**(11), 15517–15527.
7 J. C. C. Yeo, J. K. Muiruri, W. Thitsartarn, Z. Li and C. He, Recent advances in the development of biodegradable PHB-based toughening materials: Approaches, advantages and applications, *Mater. Sci. Eng., C*, 2018, **92**, 1092–1116.
8 J. C. C. Yeo, J. K. Muiruri, J. J. Koh, W. Thitsartarn, X. Zhang, J. Kong, T. T. Lin, Z. Li and C. He, Bend, twist, and turn: first bendable and malleable toughened PLA green composites, *Adv. Funct. Mater.*, 2020, **30**(30), 2001565.

 

9 M. Koller, Established and advanced approaches for recovery of microbial polyhydroxyalkanoate (PHA) biopolyesters from surrounding microbial biomass, *EuroBiotech J.*, 2020, **4**(3), 113–126.
10 C. Pérez-Rivero, J. P. López-Gómez and I. Roy, A sustainable approach for the downstream processing of bacterial polyhydroxyalkanoates: state-of-the-art and latest developments, *Biochem. Eng. J.*, 2019, **150**, 107283.
11 L. M. de Souza Mesquita, M. Martins, L. P. Pisani, S. P. Ventura and V. V. de Rosso, Insights on the use of alternative solvents and technologies to recover bio-based food pigments, *Compr. Rev. Food Sci. Food Saf.*, 2021, **20**(1), 787–818.
12 K. Papchenko, M. Degli Esposti, M. Minelli, P. Fabbri, D. Morselli and M. G. De Angelis, New sustainable routes for gas separation membranes: The properties of poly (hydroxybutyrate-co-hydroxyvalerate) cast from green solvents, *J. Membr. Sci.*, 2022, 120847.
13 G. Sed, A. Cicci, P. G. Jessop and M. Bravi, A novel switchable-hydrophilicity, natural deep eutectic solvent (NaDES)-based system for bio-safe biorefinery, *RSC Adv.*, 2018, **8**(65), 37092–37097.
14 J. Zhang and M. J. Cran, Production of polyhydroxyalkanoate nanoparticles using a green solvent, *J. Appl. Polym. Sci.*, 2022, **139**(23), 52319.
15 P. Anbukarasu, D. Sauvageau and A. Elias, Tuning the properties of polyhydroxybutyrate films using acetic acid via solvent casting, *Sci. Rep.*, 2015, **5**(1), 1–14.
16 R. A. Sequeira, S. Dubey, M. M. Pereira, T. K. Maity, S. Singh, S. Mishra and K. Prasad, Neoteric solvent systems as sustainable media for dissolution and film preparation of Poly-[(R)-3-hydroxybutyrate], *ACS Sustainable Chem. Eng.*, 2020, **8**(32), 12005–12013.
17 S. Dubey, P. Bharmoria, P. S. Gehlot, V. Agrawal, A. Kumar and S. Mishra, 1-Ethyl-3-methylimidazolium diethylphosphate based extraction of bioplastic "Polyhydroxyalkanoates" from bacteria: Green and Sustainable Approach, *ACS Sustainable Chem. Eng.*, 2018, **6**(1), 766–773.
18 Y. Chen and T. Mu, Revisiting greenness of ionic liquids and deep eutectic solvents, *Green Chem. Eng.*, 2021, **2**(2), 174–186.
19 M. P. Heaney, L. Adhikari, A. L. Siegel, K. B. Pekar, J. B. Lefton, C. McGuire, P. Rungthanaphatsophon, J. R. Walensky, G. A. Baker and T. Runčevski, Deep eutectic solvents comprising creatine and citric acid and their hydrated mixtures, *Chem. Commun.*, 2022, **58**(17), 2838–2841.
20 A. P. Abbott, G. Capper, D. L. Davies, R. K. Rasheed and V. Tambyrajah, Novel solvent properties of choline chloride/urea mixtures, *Chem. Commun.*, 2003, 70–71.
21 A. P. Abbott, D. Boothby, G. Capper, D. L. Davies and R. K. Rasheed, Deep eutectic solvents formed between choline chloride and carboxylic acids: versatile alternatives to ionic liquids, *J. Am. Chem. Soc.*, 2004, **126**(29), 9142–9147.
22 E. L. Smith, A. P. Abbott and K. S. Ryder, Deep eutectic solvents (DESs) and their applications, *Chem. Rev.*, 2014, **114**(21), 11060–11082.
23 F. M. Perna, P. Vitale and V. Capriati, Deep eutectic solvents and their applications as green solvents, *Curr. Opin. Green Sustain. Chem.*, 2020, **21**, 27–33.
24 Y. H. Choi, J. van Spronsen, Y. Dai, M. Verberne, F. Hollmann, I. W. Arends, G.-J. Witkamp and R. Verpoorte, Are natural deep eutectic solvents the missing link in understanding cellular metabolism and physiology?, *Plant Physiol.*, 2011, **156**(4), 1701–1705.
25 M. L. Picchio, D. Minudri, D. Mantione, M. Criado-Gonzalez, G. Guzmán-González, R. Schmarsow, A. J. Müller, L. C. Tomé, R. J. Minari and D. Mecerreyes, Natural Deep Eutectic Solvents Based on Choline Chloride and Phenolic Compounds as Efficient Bioadhesives and Corrosion Protectors, *ACS Sustainable Chem. Eng.*, 2022, **10**(25), 8135–8142.
26 G. Cui, X. Yang, Z. Liu, M. Wei, T. Liu, H. Gu and L. Yang, Potential Use of Limonene as an Alternative Solvent for Extraction of Gutta-Percha from Eucommia ulmoides, *ACS Sustainable Chem. Eng.*, 2022, **10**(33), 11057–11068.
27 C. Mangeon, L. Michely, A. Rios de Anda, F. Thevenieau, E. Renard and V. Langlois, Natural terpenes used as plasticizers for poly(3-hydroxybutyrate), *ACS Sustainable Chem. Eng.*, 2018, **6**(12), 16160–16168.
28 S. C. Pestana, J. N. Machado, R. D. Pinto, B. D. Ribeiro and I. M. Marrucho, Natural eutectic solvents for sustainable recycling of poly(ethyleneterephthalate): closing the circle, *Green Chem.*, 2021, **23**(23), 9460–9464.
29 M. Sharifi-Rad, E. M. Varoni, M. Iriti, M. Martorell, W. N. Setzer, M. del Mar Contreras, B. Salehi, A. Soltani-Nejad, S. Rajabi and M. Tajbakhsh, Carvacrol and human health: A comprehensive review, *Phytother. Res.*, 2018, **32**(9), 1675–1687.
30 Y. Chang, L. McLandsborough and D. J. McClements, Physicochemical properties and antimicrobial efficacy of carvacrol nanoemulsions formed by spontaneous emulsification, *J. Agric. Food Chem.*, 2013, **61**(37), 8906–8913.
31 F. Shahidi and P. Ambigaipalan, Phenolics and polyphenolics in foods, beverages and spices: Antioxidant activity and health effects – A review, *J. Funct. Foods*, 2015, **18**, 820–897.
32 J. R. Lima-de-Souza, P. R. de Oliveira, L. A. Anholeto, L. F. Sodelli, A. R. F. Ferreira, R. N. Remedio and M. I. Camargo-Mathias, The bioactive compound carvacrol as a potential acaricide: An assessment of its effects on the integument of female Rhipicephalus sanguineus sensu lato ticks, *Microsc. Res. Tech.*, 2022, **85**(5), 1784–1790.
33 A. Ultee, M. Bennik and R. Moezelaar, The phenolic hydroxyl group of carvacrol is essential for action against the food-borne pathogen Bacillus cereus, *Appl. Environ. Microbiol.*, 2002, **68**(4), 1561–1568.
34 J. Wang, R. M. Wolf, J. W. Caldwell, P. A. Kollman and D. A. Case, Development and testing of a general amber force field, *J. Comput. Chem.*, 2004, **25**(9), 1157–1174.

35 A. D. Glova, S. G. Falkovich, D. I. Dmitrienko, A. V. Lyulin, S. V. Larin, V. M. Nazarychev, M. Karttunen and S. V. Lyulin, Scale-Dependent Miscibility of Polylactide and Polyhydroxybutyrate: Molecular Dynamics Simulations, *Macromolecules*, 2018, **51**(2), 552–563.

36 C. M. Natal, M. J. G. Fernandes, N. F. S. Pinto, R. B. Pereira, T. F. Vieira, A. R. O. Rodrigues, D. M. Pereira, S. F. Sousa, A. G. Fortes, E. M. S. Castanheira and M. S. T. Gonçalves, New carvacrol and thymol derivatives as potential insecticides: synthesis, biological activity, computational studies and nanoencapsulation, *RSC Adv.*, 2021, **11**(54), 34024–34035.

37 M. D. Hanwell, D. E. Curtis, D. C. Lonie, T. Vandermeersch, E. Zurek and G. R. Hutchison, Avogadro: an advanced semantic chemical editor, visualization, and analysis platform, *J. Cheminf.*, 2012, **4**(1), 17.

38 L. Martínez, R. Andrade, E. G. Birgin and J. M. Martínez, PACKMOL: A package for building initial configurations for molecular dynamics simulations, *J. Comput. Chem.*, 2009, **30**(13), 2157–2164.

39 H. Bekker, H. J. C. Berendsen, E. J. Dijkstra, S. Achterop, R. Vondrumen, D. Vanderspoel, A. Sijbers, H. Keegstra and M. K. R. Renardus, GROMACS – A Parallel Computer For Molecular-Dynamics Simulations, in *4th International Conference on Computational Physics (PC 92)*, ed. R. A. DeGroot and J. Nadrchal, World Scientific Publishing, Singapore, 1993, pp. 252–256.

40 M. L. Picchio, D. Minudri, D. Mantione, M. Criado-Gonzalez, G. Guzmán-González, R. Schmarsow, A. J. Müller, L. C. Tomé, R. J. Minari and D. Mecerreyes, Natural Deep Eutectic Solvents Based on Choline Chloride and Phenolic Compounds as Efficient Bioadhesives and Corrosion Protectors, *ACS Sustainable Chem. Eng.*, 2022, **10**(25), 8135–8142.

41 F. Luzi, F. Dominici, I. Armentano, E. Fortunati, N. Burgos, S. Fiori, A. Jiménez, J. M. Kenny and L. Torre, Combined effect of cellulose nanocrystals, carvacrol and oligomeric lactic acid in PLA_PHB polymeric films, *Carbohydr. Polym.*, 2019, **223**, 115131.

42 B. A. Miller-Chou and J. L. Koenig, A review of polymer dissolution, *Prog. Polym. Sci.*, 2003, **28**(8), 1223–1270.

43 N. A. Peppas, J. Wu and E. D. von Meerwall, Mathematical modeling and experimental characterization of polymer dissolution, *Macromolecules*, 1994, **27**(20), 5626–5638.

44 N. Yabueng and S. C. Napathorn, Toward non-toxic and simple recovery process of poly(3-hydroxybutyrate) using the green solvent 1,3-dioxolane, *Process Biochem.*, 2018, **69**, 197–207.

45 A. Aramvash, N. Gholami-Banadkuki, F. Moazzeni-Zavareh and S. Hajizadeh-Turchi, An environmentally friendly and efficient method for extraction of PHB biopolymer with non-halogenated solvents, *J. Microbiol. Biotechnol.*, 2015, **25**(11), 1936–1943.

46 V. Elhami, N. van de Beek, L. Wang, S. J. Picken, J. Tamis, J. A. Sousa, M. A. Hempenius and B. Schuur, Extraction of low molecular weight polyhydroxyalkanoates from mixed microbial cultures using bio-based solvents, *Sep. Purif. Technol.*, 2022, **299**, 121773.

47 B. Mongili, A. Abdel Azim, S. Fraterrigo Garofalo, E. Batuecas, A. Re, S. Bocchini and D. Fino, Novel insights in dimethyl carbonate-based extraction of polyhydroxybutyrate (PHB), *Biotechnol. Biofuels*, 2021, **14**, 1–16.

48 S. Alfano, L. Lorini, M. Majone, F. Sciubba, F. Valentino and A. Martinelli, Ethylic esters as green solvents for the extraction of intracellular polyhydroxyalkanoates produced by mixed microbial culture, *Polymers*, 2021, **13**(16), 2789.

49 P. Klinmalai, A. Srisa, Y. Laorenza, W. Katekhong and N. Harnkarnsujarit, Antifungal and plasticization effects of carvacrol in biodegradable poly(lactic acid) and poly(butylene adipate terephthalate) blend films for bakery packaging, *LWT*, 2021, **152**, 112356.

50 J. Andrade, C. González-Martínez and A. Chiralt, Effect of carvacrol in the properties of films based on poly(vinyl alcohol) with different molecular characteristics, *Polym. Degrad. Stab.*, 2020, **179**, 109282.

51 X. Hou, S. Liu and C. He, Designing ultratough, malleable and foldable biocomposites for robust green electronic devices, *J. Mater. Chem. A*, 2022, **10**(3), 1497–1505.

52 S. Pradhan, P. K. Dikshit and V. S. Moholkar, Production, ultrasonic extraction, and characterization of poly(3-hydroxybutyrate) (PHB) using Bacillus megaterium and Cupriavidus necator, *Polym. Adv. Technol.*, 2018, **29**(8), 2392–2400.

53 R. G. Hill, Biomedical polymers, *Biomaterials, artificial organs and tissue engineering*, Elsevier, 2005, pp. 97–106.

54 H. Sato, Y. Ando, J. Dybal, T. Iwata, I. Noda and Y. Ozaki, Crystal Structures, Thermal Behaviors, and C–H···O═C Hydrogen Bondings of Poly(3-hydroxyvalerate) and Poly(3-hydroxybutyrate) Studied by Infrared Spectroscopy and X-ray Diffraction, *Macromolecules*, 2008, **41**(12), 4305–4312.

55 G. S. Kiran, S. A. Jackson, S. Priyadharsini, A. D. Dobson and J. Selvin, Synthesis of Nm-PHB (nanomelanin-polyhydroxy butyrate) nanocomposite film and its protective effect against biofilm-forming multi drug resistant Staphylococcus aureus, *Sci. Rep.*, 2017, **7**(1), 1–13.

56 S. L. De Rooy, E. T. Wahyuni, W. Wiratni, S. Syamsiah and J. Ismail, Purification and characterization of poly-hydroxybutyrate (PHB) in Cupriavidus necator, *Indones. J. Chem.*, 2007, **7**(3), 243–248.

57 S. A. Andaloussi, D. L. Versace, E. Renard, E. Dessauw and V. Langlois, Electrospun Nanofibrous Poly(3-Hydroxybutyrate-Co-3-Hydroxyvalerate) With Antibacterial Activity, *J. Bio. Engineer. Med.*, 2019, **1**(1), 2–7.

58 E. P. Chang, Viscoelastic Properties of Pressure-Sensitive Adhesives, *J. Adhes.*, 1997, **60**(1–4), 233–248.

59 B. Al-Shammari, T. Al-Fariss, F. Al-Sewailm and R. Elleithy, The effect of polymer concentration and temperature on the rheological behavior of metallocene linear low density polyethylene (mLLDPE) solutions, *J. King Saud Univ., Eng. Sci.*, 2011, **23**(1), 9–14.

60 Q. Liao, I. Noda and C. W. Frank, Melt viscoelasticity of biodegradable poly(3-hydroxybutyrate-co-3-hydroxyhexanoate) copolymers, *Polymer*, 2009, **50**(25), 6139–6148.

 

61 A. Rios de Anda, P. Sotta, T. Modjinou, V. Langlois, D.-L. Versace and E. Renard, Multiscale Structural Characterization of Biobased Diallyl–Eugenol Polymer Networks, *Macromolecules*, 2020, **53**(6), 2187–2197.

62 R. Barbas, R. Prohens, M. Font-Bardia, A. Bauzá and A. Frontera, Hydrogen bonding versus π-interactions: their key competition in sildenafil solvates, *CrystEngComm*, 2018, **20**(32), 4526–4530.

63 G. Sivasankarapillai, E. Eslami and M.-P. Laborie, Potential of organosolv lignin based materials in pressure sensitive adhesive applications, *ACS Sustainable Chem. Eng.*, 2019, **7**(15), 12817–12824.

64 A. J. Sandoval, M. M. Fernández, M. V. Candal, M. Safari, A. Santamaria and A. J. Müller, Rheology and Tack Properties of Biodegradable Isodimorphic Poly(butylene succinate)-Ran-Poly(ε-caprolactone) Random Copolyesters and Their Potential Use as Adhesives, *Polymers*, 2022, **14**(3), 623.

65 Y. Lin, M. Ye, X. Zhang, Y. Chen, Y. Chen, J. Wu and H. Wang, Biodegradable copolyesters based on a "soft" isohexide building block with tunable viscoelasticity and self-adhesiveness, *Polym. Chem.*, 2022, **13**(31), 4511–4523.

66 T. T. D. Chen, L. P. Carrodeguas, G. S. Sulley, G. L. Gregory and C. K. Williams, Bio-based and Degradable Block Polyester Pressure-Sensitive Adhesives, *Angew. Chem., Int. Ed.*, 2020, **59**(52), 23450–23455.

67 M. A. Droesbeke, A. Simula, J. M. Asua and F. E. Du Prez, Biosourced terpenoids for the development of sustainable acrylic pressure-sensitive adhesives via emulsion polymerisation, *Green Chem.*, 2020, **22**(14), 4561–4569.

68 F. Deplace, C. Carelli, S. Mariot, H. Retsos, A. Chateauminois, K. Ouzineb and C. Creton, Fine Tuning the Adhesive Properties of a Soft Nanostructured Adhesive with Rheological Measurements, *J. Adhes.*, 2009, **85**(1), 18–54.

69 X. Callies, C. Fonteneau, S. Pensec, L. Bouteiller, G. Ducouret and C. Creton, Adhesion and non-linear rheology of adhesives with supramolecular crosslinking points, *Soft Matter*, 2016, **12**(34), 7174–7185.

70 H. Wang and K. Tashiro, Reinvestigation of crystal structure and intermolecular interactions of biodegradable poly (3-hydroxybutyrate) α-form and the prediction of its mechanical property, *Macromolecules*, 2016, **49**(2), 581–594.

71 Y. Doi, M. Kunioka, Y. Nakamura and K. Soga, Nuclear magnetic resonance studies on poly(β-hydroxybutyrate) and a copolyester of β-hydroxybutyrate and β-hydroxyvalerate isolated from Alcaligenes eutrophus H16, *Macromolecules*, 1986, **19**(11), 2860–2864.

72 H. D. Özeren, M. Guivier, R. T. Olsson, F. Nilsson and M. S. Hedenqvist, Ranking Plasticizers for Polymers with Atomistic Simulations: PVT, Mechanical Properties, and the Role of Hydrogen Bonding in Thermoplastic Starch, *ACS Appl. Polym. Mater.*, 2020, **2**(5), 2016–2026.